Optical and hygroscopic properties of black carbon influenced by particle microphysics at the top of anthropogenically polluted boundary layer

Shuo Ding[1], Dantong Liu[1], Delong Zhao[2,3], Kang Hu[1], Ping Tian[2,3], Fei Wang[2], Ruijie Li[2], Yichen Chen[2], Hui He[2], Mengyu Huang[2], Deping Ding[2]

[1]Department of Atmospheric Sciences, School of Earth Sciences, Zhejiang University, Hangzhou, China

[2]Beijing Weather Modification Office, Beijing, China

[3]Beijing Key Laboratory of Cloud, Precipitation and Atmospheric Water Resources, Beijing, China

Corresponding to: dantongliu@zju.edu.cn

Abstract

Aerosols at the top of planetary boundary layer (PBL) could modify its atmospheric dynamics by redistributing the solar radiation, and start to be activated to form low-level cloud at this layer. Black carbon (BC), as an aerosol component efficiently absorbing solar radiation, can introduce heating and positive radiative effects at this sensitive layer, especially in the polluted PBL over the continent. This study presents continuous measurements of detailed BC properties at a mountain site locating at the top of polluted PBL over the North China Plain, during seasons (3 and 4 weeks of data during winter and summer, respectively) with contrast emission structure and meteorology. The pollution level was persistently influenced by local surface anthropogenic emission on daily basis through daytime convective mixing, but the concentration was also enhanced or diluted depending on air mass direction, defined as neutral, polluted and diluted PBL, respectively. Winter was observed to have a higher BC mass fraction (4-8%) than summer (2-7%). By resolving the detailed particle size-resolved mixing state of BC in optical and hygroscopic models, we found enhanced BC mass absorption cross section (MAC_{BC}) for polluted PBL (up to 13 m^2g^{-1} at λ=550 nm), which was 5% higher during summer than winter due to smaller BC core size. The higher BC mass fraction in winter corresponded with a lower single-scattering albedo by 0.03- 0.09 than summer, especially the lowest for diluted winter PBL (0.86±0.02). The water supersaturation (SS) required to activate half number of BC decreased from 0.21±0.08% to 0.1±0.03% for winter diluted and polluted PBL; from 0.22±0.06% to 0.17±0.05% for summer. Notably, at the top of anthropogenically polluted PBL in both seasons, the enlarged BC with enhanced absorption capacity could be also efficiently droplet activated, e.g. winter (summer) BC with MAC of 9.84±1.2 (10.7±1) $m^2 \cdot g^{-1}$ could be half activated at SS=0.13±0.06% (0.18±0.05%). These BC at the top of the PBL can more directly interact with the free troposphere and be transported to a wider region, exerting important direct and indirect radiative impacts.

1. Introduction

Black carbon aerosol (BC) is strongly shortwave absorbing, wielding important climate warming impact in regional and global scale (Bond et al., 2013;Bond and Bergstrom, 2006). The emission of BC has large regional heterogeneity with higher impact over polluted regions (Ramanathan and Carmichael, 2008). The impacts due to BC heating are importantly determined by its vertical distribution in atmospheric column, which could lead to a more stable or convective planetary boundary layer (PBL) (Ding et al., 2016;Koch and Del Genio, 2010), e.g. an enhanced heating at higher level will depress the development of the layer below (Chung et al., 2002;Ramanathan et al., 2005;Hansen et al., 2005), while the heating can promote the convection above (Mcfarquhar and Wang, 2006;Rudich et al., 2003), e.g. BC was found to account for 43% of the total aerosol radiative forcing at the atmosphere in south Asia due to heating (Raju et al., 2020). Therefore, the properties of BC at the top of PBL are important, which may result in contrast impacts in perturbing atmospheric dynamics. In addition, surface emissions could serve regular cloud condensation nuclei (CCN) on daily basis through daytime convective mixing in the PBL (Bretherton and Wyant, 1997;Wood and Bretherton, 2004). Aerosols can be uplifted to the top of PBL and subsequently activated to incorporate into clouds. However, the way of BC from surface sources to be activated, after the PBL processing during vertical transport, is yet to be explicitly understood.

Ground measurements of BC have been intensively conducted over the polluted North China Plain (NCP) region in last decades (Han et al., 2009;Cheng et al., 2011;Ji et al., 2018;Liu et al., 2019a), e.g. the seasonal variation of elemental carbon in urban Beijing during 2005-2006 and 2012-2013 (Han et al., 2009;Ji et al., 2018), the size-resolved mixing state of BC and aging mechanism at a suburban site in NCP (Cheng et al., 2011), and the contrast physical properties in urban Beijing between winter and summer (Liu et al., 2019a), were investigated in these studies. But these results were not able to represent the BC properties at the top of PBL. Additionally, recently conducted series of aircraft measurements provided comprehensive information about vertical distributions of BC over this region (Zhao et al., 2019;Ding et al., 2019a), but the manner of the aircraft measurement could not capture the variation of BC at certain level in sufficient time resolution. The nature of diurnal pattern of PBL means not only the surface concentration of pollutants is influenced by the daily evolution of PBL, but also the pollutants at the top of PBL will have diurnal variation which need stable measurements to be characterized. This is particularly the case if the top of PBL was continuously influenced by surface emissions. However such information is lack at the top of PBL over the polluted NCP region, and many models still reply on surface measurements to estimate the conditions at higher level (Guleria et al., 2014;Srivastava et al., 2012a).

Microphysical properties of BC importantly determine its optical and hygroscopic properties. For example, the presence of coatings associated with refractory BC (rBC) may enhance its absorbing capacity (Liu et al., 2017), also enhances its hygroscopicity (Liu et al., 2013) and particle size, thereby modifying the potential to be droplet activated (Chuang et al., 2002;Panicker et al., 2016;Ding et al., 2019b). This study is for the first time to characterize the detailed BC microphysics at a mountain site located at the top of PBL, influenced by surface emission on daily basis over the NCP region. We have conducted the experiments with intensive measurements lasting for one month for each of the representative seasons. We investigated the optical and hygroscopic properties of BC at this level, as influenced by microphysical properties. Such information will support to constrain the impacts of BC in influencing the PBL dynamics and low-level cloud formation over this anthropogenically polluted region.

2. Site description, meteorology, cluster classification

Experiments in this study were performed in winter (Feb. - Mar.) and summer (Jun. – Jul.) of 2019 at a mountain site (115.78°E, 40.52°N, 1344 m), locating on the north of Taihang ridge to the northwest of central Beijing, shown in Fig 1. (a). The site is away from any local primary emissions, but the only sources of pollutants are contributed by lower-level surface emissions and regional transport (the follow-up discussions).

Backward trajectories at the site are analyzed using the HYSPLIT 4.0 model (Draxler and Hess, 1998), for every 6-hour during the experimental period. The meteorological field uses the 1° × 1°, 3-hourly GDAS1 reanalysis product and trajectories back to 48h are calculated. The backward trajectories are used for further cluster analysis, to group the backward trajectories with similar transport pathway, whereby the homogeneity of trajectories is maximized in each cluster, meanwhile the heterogeneity among different clusters is maximized (Makra et al., 2011). This is achieved by analyzing the spatial variance of each trajectory and the total variance in each pre-defined cluster. The iteration next simultaneously calculates and assigns the trajectories to the eventually merged clusters. This analysis has been widely used to identify the main transport pathways of air mass (Markou and Kassomenos, 2010;Philipp, 2009;Jorba et al., 2004;Grivas et al., 2008), and is performed using the built-in module in HYSPLIT model software.

3. Instrumentation

All aerosol measurements were performed behind a $PM_{2.5}$ impactor (BGI SCC1.829), and were dried by a Nafion tube prior to the sampling of the instruments. BC was measured by a single-particle soot photometer (SP2) (DMT Inc. USA). This instrument uses laser-induced technique to incandesce BC-containing particle (Schwarz et al., 2006;Liu et al., 2010). The measured incandescence signal of individual BC particle can be converted to a refractory BC (rBC) mass, which was calibrated using Aquadag® BC particle standard (Acheson Inc.), and a factor of 0.75 was applied to correct for the ambient rBC mass (Laborde et al., 2012). The core size (D_c) of BC is calculated from the measured rBC mass by assuming a material density of BC of 1.8 g/cm^3 (Bond and Bergstrom, 2006). The scattering cross section of BC is derived by the leading edge only (LEO) method (Gao et al., 2007) on the measured scattering signal of individual BC particle. The entire particle size of BC-containing particle (D_p) including coatings is determined by matching the measured scattering cross section with the modelled one based on core-shell assumption using a Mie lookup table (Liu et al., 2014;Taylor et al., 2015). This assumption is mostly valid for BC with thick coatings (Liu et al., 2017), but not considering the scenario in which BC may be attached to dust particle (Srivastava et al., 2018), given there was no dust event observed in this study. The bulk coating thickness (D_p/D_c) in a given time window is calculated as the cubic root of the total volume of BC-containing particle weighted by the total volume of rBC (Liu et al., 2014):

$$\frac{D_p}{D_c} = \sqrt[3]{\frac{\sum_i D_{p,i}^3}{\sum_i D_{c,i}^3}} \qquad (1),$$

where $D_{p,i}$ and $D_{c,i}$ are the diameters for the ith single particle, respectively. The count (or mass) median diameter (CMD, or MMD) is derived from a number (or mass) size distribution, below and above which size the number (or mass) concentration is equal. Modelled mass absorption cross section (MAC) of individual BC-containing particle is calculated by applying the Mie theory (Bohren, 1998) with a core-shell mixing state assumption. The bulk MAC for a given time window can then be determined by the total MAC of each BC particle divided by the total rBC mass, expressed as:

$$MAC = \frac{\sum_i MAC_i \times m_{rBC,i}}{\sum_i m_{rBC,i}} \qquad (2),$$

where MAC_i and $m_{rBC,i}$ is the MAC and rBC mass for each particle respectively. An example to calculate the MAC from single particle information is shown in Fig. 5f. The absorption coefficient k_{abs} (in Mm^{-1}) is

calculated as the MAC ($m^2 \cdot g^{-1}$) multiplying the rBC mass concentration ($\mu g \cdot m^{-3}$) in each size bin, then integrated throughout the size distribution:

$$k_{abs} = \sum_i MAC(D_{p,i}, D_{c,i}) m(logD_{c,i}) \Delta logD_{c,i} \quad (3),$$

where m ($logD_{c,i}$) is the BC mass concentration at each D_c bin.

the volume ratio between coating and rBC could be obtained from D_c and D_p of individual BC:

$$\frac{\varepsilon_{coating}}{\varepsilon_{rBC}} = \left(\frac{D_p}{D_c}\right)^3 - 1 \quad (4),$$

where $\varepsilon_{coating}$ and ε_{rBC} is the volume fraction within BC particle. The hygroscopicity parameter of BC (κ_{BCc}) could be calculated with known $\kappa_{coating}$ and κ_{rBC}=0, based on Zdanovskii–Stokes–Robinson (ZSR) rule (Stokes and Robinson, 1966), expressed as,

$$\kappa_{BCc} = \varepsilon_{coating} \times \kappa_{coating} \quad (5),$$

In this study, the main focus is the coating abundance distribution across all BC size distribution, but the variation of coating composition is to a less importance, thus a constant $\kappa_{coating}$=0.3 is used to represent typical environment containing aged aerosols (Pringle et al., 2010). An example to calculate κ_{rBC} from single particle information is shown in Fig. 5g.

Total aerosol size distribution was measured by a Scanning Mobility Particle Size (SMPS, TSI Inc. Model 3936) at mobility diameter 15-700 nm. The total particle mass below diameter 1 μm (PM_1) is derived from the SMPS size distribution by assuming a mean particle density of 1.45 g cm^{-3} (Liu et al., 2015;Cross and et al., 2007). The scattering cross-section σ_{sc} (μm^2) of particle at all sizes is calculated by applying Mie calculation assuming a refractive index (RI) of 1.48+0i (Liu et al., 2009) (a positive imaginary RI considering the BC mass fraction is tested to have a minor influence in total scattering within 3%), thereby calculating the scattering coefficient k_{sca} (in Mm^{-1}) of all aerosols:

$$k_{sca} = \sum_i \sigma_{sc}(D_i) n(logD_i) \Delta logD_i \quad (6),$$

where n ($logD_i$) represents the particle number concentration at the ith size bin. Single-scattering albedo (SSA) is derived as the quotient of scattering coefficient (k_{sca}) divided by extinction coefficient (k_{abs}+ k_{sca}).

4. Results and discussion

4.1 Classification of PBL

Clustered air masses for both seasons are shown in Fig. 2, and three clusters are classified for each season. For both seasons, Cluster 1 (C1) represents the air masses from the most intensive anthropogenically influenced regions according to the BC emission inventory (Fig. 1b). The seasonal difference is the winter pollution was transported from the west over Shanxi and Hebei province, while was southerly in summer mainly from the North China Plain over Hebei province. Cluster 2 (C2) passed over similar regions in both seasons from the cleaner north. Cluster 3 (C3) both had a longer transport than other clusters, from northwest and northeast in winter and summer respectively. The diurnal variations of PBL height (PBLH) corresponding with periods of each cluster are shown in Fig. 2(d, h), with pronounced diurnal pattern. Apart from C3, winter had a lower PBLH than summer, i.e. the mountain site was slightly above or below the well-developed PBL top in winter and summer, respectively. The consistent diurnal variation of PBL means the mountain site was persistently influenced by the surface sources through daytime convective mixing, when pollutants were transported in the polluted PBL. However, the actual concentration will depend whether the site had been contributed by additional sources or dilution (Fig. 1c).

Fig. 3 shows the temporal evolution of BC mass and PM for both seasons classified by air mass clusters, with right panels showing the frequency under each cluster. Fig. 4 shows their diurnal variations. For all experimental period, the concentration level of BC mass generally positively correlated with the PM mass, both indicating the pollution levels. Among the three clusters, C2 had the medium mass concentration, with over 85% frequency of the air masses contributed by local regions (±1° around the measurement site), and additional air masses were from the cleaner northerly direction, similar for both seasons (Fig. 2). It is likely that this cluster was mainly contributed by local emission, and occasionally diluted to some extent by the air mass from less polluted region. Here this cluster is defined as "neutral PBL", to be discriminated with the other two clusters. In winter C2 showed clear diurnal variation of BC and PM_1 concentration with significant enhancement in the daytime (Fig. 4b and e) when fully developed PBL (Fig. 2d), with the diurnal pattern consistent with a previous study conducted in the Indian Himalayan foothills (Srivastava et al., 2012b) . This diurnal pattern on the mountain was contrast with the usual surface measurement, when the daytime PBL development could dilute the concentration (Liu et al., 2019a;Han et al., 2009). This opposite trend on the mountain site was consistent with the fully developed PBLH at 12:00-16:00 (Fig. 2d) when the top of PBL reached the mountain site at this time, and pollutants were transported through convective mixing from the surface sources (Fig. 1c). In midnight, the nocturnal depressed PBL trapped the surface pollution towards mountain, and the subsiding cleaner air in free troposphere may have diluted the concentration of pollutants on the mountain site (Sullivan et al., 1998;Bennett et al., 2010). The enhanced concentration from midday in summer was also observed (on the mean, Fig. 4a) but not as pronounced as winter, probably due to some wet removal during the daytime vertical transport from the surface, given the high RH in the summer (Fig. S1).

Consistent with the combined back-trajectory and emission analysis above, C1 had for both seasons the highest BC (1.0 ± 0.5 and 0.4±0.2 μg m^{-3} for winter and summer, respectively) and highest PM mass (23.8 ± 10.3 and 13.4±9.5 μg m^{-3}). Compared to C1, for C2, the concentration of BC mass was enhanced by a factor of 2.8 (1.7) higher than that in C2 for winter (summer), with winter having mass concentration frequently exceeding 1 μg m^{-3}. C1 clearly shows the diminished diurnal variation compared to the neutral PBL of C2, but all increased throughout the day and night (Fig. 4a and d), particularly for winter. This is because besides the persistent influence of daytime convective mixing as the neutral cluster in C2, C1 cluster had additional contribution from wider polluted regions, hereby defined as "polluted PBL" (Fig. 1c). This contribution by regional transport was not related to a diurnal pattern. The less concentration in summer mountain may also result from the lower surface emission in the season.

C3 had the lowest pollution level among all air mass clusters with a lower BC (0.09±0.03 μg m^{-3}) and PM_1 mass (1.8±0.4 μg m^{-3}) than C2 by a factor of 2-4, within a similar range of a previous study in western and central Himalayas (Nair et al., 2013). C3 represented the air masses from regions with low emissions (Fig. 1b). In addition, the faster transport (shown as the longest path for back-trajectories among clusters, Fig. 2c) and the highest PBLH (Fig. 2d) in C3 could efficiently dilute the pollution in the PBL, hereby termed as "diluted PBL". Compared to C2, C3 can efficiently disperse and reduce the pollutants being vertically transported to the mountain site from the surface, thus with no apparent diurnal pattern of pollution concentrations neither (Fig. 4c).

BC mass fraction in PM_1 was overall higher in winter than summer, on average at 5.1±1.7% and 3.6±2.3% respectively, with both seasons showing a frequency distribution skewed to higher values up to 10% (Fig. 3 k and l). Note that in summer the BC mass fraction among clusters had no discernible differences with only C2 showing to be slightly higher. The overall higher BC mass fraction in winter may result from the seasonal variation on emission structure, that the additional primary emissions from heating activities may have introduced more fraction of BC (Chow et al., 2011;Liu et al., 2018). However the lowered BC mass fraction for the polluted PBL in winter (with significant reduction for fraction >7%) may result from the enhanced secondary formation under polluted environment (Volkamer et al., 2006;Hallquist et al., 2009). The

comparable BC mass fraction between C1 and C3 in summer (but all lower than neutral PBL) may result from the dominant process of enhanced secondary formation (reducing PM_1) and particle scavenging (reducing BC), for polluted and diluted PBL, respectively. There was a notably higher BC mass fraction at 6.7±1.5% for the diluted PBL in winter, suggesting a much reduced secondary aerosols in less-polluted environment, and the removal process of BC had been less efficient than other substances (Koch and Del Genio, 2010).

4.2 Particle microphysics of BC

BC core size showed no variation among all PBL types in both seasons. The mass (count) median diameter of BC core is 203±12 nm (106±7 nm) and 167±11 nm (85±5 nm) for winter and summer respectively. The BC core size could be used to discern emission sources, such as BC from solid fuel burning tended to have larger MMD compared to those from traffic sources (Liu et al., 2014). The larger MMD in winter than summer was consistent with previous observation over this region (Ding et al., 2019a;Hu et al., 2020), which may indicate additional sources from residential solid fuel burning for heating in cold season.

The coatings relative to BC, as reflected by D_p/D_c, was positively correlated with the pollution level of the PBL (represented by PM_1 mass loading) in winter (Fig. 5a), and in summer from neutral to polluted PBL (Fig. 5b). The polluted PBL in winter had the highest D_p/D_c (1.76 ±0.3), in line with the most polluted condition. For both neutral and diluted PBL, winter had higher BC coatings than summer. Apart from some periods in summer, the diluted PBL occasionally showed higher D_p/D_c up to 1.8, comparable with the high end of that for polluted PBL.

The warmer temperature in summer may have caused a more likely tendency for some semi-volatile particle species to evaporate, hereby reduced coatings on BC than in winter even at the same pollution level, which is consistent with previous ground studies over this region (Liu et al., 2019a). The highest coatings were associated with the most polluted condition, implying that the regional transport of air mass from wider polluted region may have advected both primary emissions and gas-precursors, during when some gas partitioning processes may have occurred on BC during transport and caused the high coatings. Under clean environment, summer showed remarkably higher coatings than winter, which may result from a more intense solar radiation received at the mountain site in summer, where photochemical reactions may have caused significant formation of secondary particulate matter (Xu et al., 2017;Bao et al., 2018;Liu et al., 2019b).

The detailed size distributions of uncoated and coated BC are shown in Fig. 5 c-e. Here three typical examples are chosen to represent the polluted and diluted PBL in winter (case 1 and case 2), and polluted PBL in summer (case 3). Comparing between case 1 and case 2, it showed the polluted period had caused increased size for all particle from peak diameter (d) less than d=30 nm to the accumulation mode of d=120 nm. Coated BC diameter peaked from 150 to 220 nm. It means the condensation process had occurred on all particles and enlarged their sizes including BC. The coated BC in most polluted PBL has significantly extended its coated size up to d=400-700nm. Note that for the clean PBL in winter, the coated BC was populated at d=150nm, leading to a higher BC number fraction of 22% at this size. For polluted PBL in summer, peaking diameter of all particles (d=450nm) was lower than winter, and coated BC also peaked at a smaller size (d=153 nm). Fig. S3 shows almost consistent coated BC sizes in summer (120-130nm), which was smaller than winter because of the smaller core size (though a higher D_p/D_c).

Detailed core-size resolved mixing states, expressed in a space of coated versus uncoated BC diameter, are shown in Fig. 5 f-h, corresponding to the three cases above. $D_p=D_c$ indicates no coatings on BC and coating increases when D_p is larger than D_c. For polluted PBL in winter, most BC population lied between 100-200 nm core diameter and 200-300 nm coated diameter, in contrast with the diluted PBL that a significant fraction of uncoated BC and coated diameter at 100-140 nm. Summer polluted PBL showed reduced fraction of bare

BC but a range of coating thickness for coated BC. Such analysis in mapping the size-resolved mixing state of single BC particle on the space of uncoated-coated size, can resolve the optical (contour in Fig. 5f) and hygroscopic (contour in Fig. 5g) properties that BC particle microphysics could influence, which will be discussed next.

4.3 Optical properties of BC

Fig. 6 a-b and Fig. S4 show the mass absorption cross section (MAC) of uncoated and coated BC for different PBL types in both seasons. Summer showed systematically higher MAC (7.2±0.1 $m^2 \cdot g^{-1}$) than winter (6.6±0.3 $m^2 \cdot g^{-1}$) for uncoated BC, because the BC core was smaller in summer than winter (Fig. S2 and Fig. S3). The MAC for coated BC was largely modulated by coatings, showing positive correlation with PM_1 in winter ($MAC_{BC,coated}$=0.09×PM_1+8.7, r=0.79) and summer ($MAC_{BC,coated}$=0.12×PM_1+9.5, r=0.5), corresponding with the diluted to polluted PBL types. The enhanced absorption efficiency of coated BC with increased pollution level was consistent with previous studies over this region (Zhang et al., 2018;Ding et al., 2019a). The mean $MAC_{BC,coated}$ for polluted PBL in summer (11±1 $m^2 \cdot g^{-1}$) was higher than that in winter (10.7±0.9 $m^2 \cdot g^{-1}$) by 2%. The neutral and diluted PBL also had higher MAC in summer than winter (by 8% and 22% respectively). The overall higher absorption efficiency of BC in summer (especially in diluted PBL) was due to the smaller core size, leading to a higher baseline MAC for uncoated BC by 10% than winter. This effect prevailed the even lower coating amount and associated absorption enhancement in summer (Fig. 5b). Notably, the MAC_{BC} for diluted summer PBL had been enhanced by both reduced BC core size and increased coatings (Fig. 5b) reaching almost equivalent MAC compared to winter neutral PBL. This means at the top of the clean PBL in summer, there was a BC layer with high absorbing capacity (in contrast to winter with much lower MAC), which may efficiently absorb the strong solar radiation.

The single-scattering albedo at λ=550nm (SSA_{550}) in winter was systematically lower for all PBL types (Fig. 6 c-d and Fig. S4), lowered by 0.06, 0.05 and 0.08 than summer for diluted, neutral and polluted PBL, respectively. The decreased SSA_{550} was in line with the increased BC mass faction (Fig. 3), and also influenced by the absorbing efficiency. Our winter results here were comparable to previous aircraft measurements over Beijing region in cold season of 2016, with SSA ranging from 0.8 to 0.98 from clean to heavily polluted period in the PBL (Tian et al., 2020). For the diluted PBL in winter, SSA_{550} could reach as low as 0.86±0.02 when BC mass fraction reached 7±1.5% (Fig. 3k). This was within the range of that study in clean period at SSA=0.8-0.85 in the PBL, and the neutral and polluted PBL were within similar range in transition and fully polluted PBL at SSA=0.85-0.98, suggesting the clusters here may represent different development stages of pollution events. The lower SSA in winter PBL than summer tended to induce radiative effects towards more positive effect (Hansen et al., 1981;Haywood and Ramaswamy, 1998) at the top of PBL, in particular for the clean winter PBL.

4.4 Hygroscopic properties of BC

The droplet activation of BC is determined by the particle size and hygroscopicity, where the coatings play roles in enlarging entire BC size (Dusek et al., 2006a;Dusek et al., 2006b) and increasing its hygroscopicity (Liu et al., 2013). Both factors can be obtained by our observation of size-solved mixing state of BC. The coated BC diameter based on number concentration (coated CMD) is shown in Fig. 7 a, b. The CMD of coated BC in winter polluted PBL was 0.19±0.05 μm, which were the largest among PBL types. Generally, coated BC CMD was in positive correlation with the PM, in winter fitted as CMD=0.003×PM_1+0.14 (r=0.69) and in summer as CMD=0.001×PM_1+0.11 (r=0.73). The coated BC CMD in winter PBL was larger than summer by 14 nm, 35 nm and 56 nm for diluted, neutral and polluted PBL, respectively.

The hygroscopicity parameter of BC-containing particle (κ_{BCc}) at the size of CMD is positively correlated with coating content. In winter κ_{BCc} was at 0.15±0.02, 0.20±0.03 and 0.24±0.03 for diluted, neutral and polluted PBL respectively, while the corresponding values were 0.19±0.03, 0.20±0.03 and 0.22±0.03 in summer, consistent with the reduced D_p/D_c from polluted PBL to diluted PBL for both seasons. κ_{BCc} could be fitted as κ_{BCc}=0.003×PM_1+0.17 (r=0.77) and κ_{BCc}=0.004×PM_1+0.17 (r=0.49) for winter and summer respectively. Note that summer diluted PBL had significantly higher κ (0.19±0.03) than winter for the same PBL type.

After obtaining the CMD of coated BC and the corresponding κ_{BCc}, a critical water superstation (SS) could be derived from the Kölher model (Fig. S5) for BC at the size of CMD to be activated. By assuming that all of the population larger than CMD could also be consequently activated (because of the larger particle size and higher hygroscopicity), the SS obtained above is thus the lower estimate for half of the number population of BC to be activated, termed as SS_{half}. In line with the increased coated BC size and particle hygroscopicity, SS_{half} decreased with increased pollution level, from 0.21±0.08% to 0.1±0.03% for winter diluted to polluted PBL; from 0.22±0.06% to 0.17±0.05% for summer. This highlights the lowest possible SS required to activate BC in polluted winter PBL, and for the same PBL type, summer will need a higher SS, apart from occasionally some lower SS_{half} for summer diluted PBL. This potential CCN ability of BC is derived from the physical properties of BC itself, but the actual activation of BC depends on the ambient superstation condition which is determined by the size distribution of existing droplets and other aerosols competing CCN (Pruppacher et al., 1998;Mcfiggans et al., 2005). The results here generally consistent with a previous surface measurement of BC CCN-activation in urban Nanjing as constrained by size-resolved compositions (Wu et al., 2019), when an activation fraction of 33% at SS=0.1% was found. Previous study using flight measurements over NCP region (Ding et al., 2019a) found a SS=0.08% required to activate half of the BC number in heavy pollution condition, consistent with the polluted PBL here.

5. Conclusion

By performing continuous measurement on a mountain site located at the top of planetary boundary layer (PBL) over the north China Plain region in winter and summer, the optical and hygroscopic properties of BC were investigated. We identified three types of PBL, all persistently influenced by surface anthropogenic emission on daily basis through daytime convective mixing, but could be either enhanced or diluted subject to received air masses. By investigating the detailed microphysical properties of BC, this study provides a clear picture of optical and hygroscopic characteristics of BC at the top of anthropogenically influenced PBL. Highlighted information includes higher BC mass fractions in winter than summer, corresponding with a lower single-scattering albedo by 0.05-0.08, especially the lowest for diluted winter PBL (0.86±0.02); both mass absorbing efficiency and CCN ability of BC are positively correlated with the pollution level of PBL, due to enhanced coating content under more polluted environment, e.g. from diluted to polluted PBL, coating content increased by 39% (11%), absorbing efficiency increased by 31% (10%), and the water supersaturation in activating half number of BC decreased by 53% (26%) for winter and summer respectively. It clearly demonstrates that BC with higher coating content could be efficiently incorporated into liquid clouds, and meanwhile these BC had high absorbing capacity, which means these highly-absorbing BC may have great potentials for in-cloud heating (Jacobson, 2012;Nenes and et al., 2002).

Compared to surface measurement, the results here are more directly linked to the aerosol properties closer to the condensation level which is subsequently CCN-activated. BC located at this layer more importantly determines its heating impacts due to receiving a stronger solar radiation. Rather than being subject to significant scavenging processes of low-level emissions, BC transported to the lower free troposphere may be transported to a wider region (Weinzierl, 2008;Yang et al., 2018b;Govardhan et al., 2017), exerting regional

direct and indirect radiative impacts.

Acknowledgment

This research was supported by the National Key Research and Development Program of China (2016YFA0602001), National Natural Science Foundation of China (41875167, 41675038).

There are no potential conflicts of interest.

The data in this study are available from the corresponding author upon request (dantongliu@zju.edu.cn).

Author Contributions

DL, DZ and DD led and designed the study. SD, DL, DZ, KH, PT, RL,YC, FW, HH, and MH set up and conducted the experiment. SD, DL and KH contributed to the data analysis. SD, DL wrote the paper.

Figures and captions

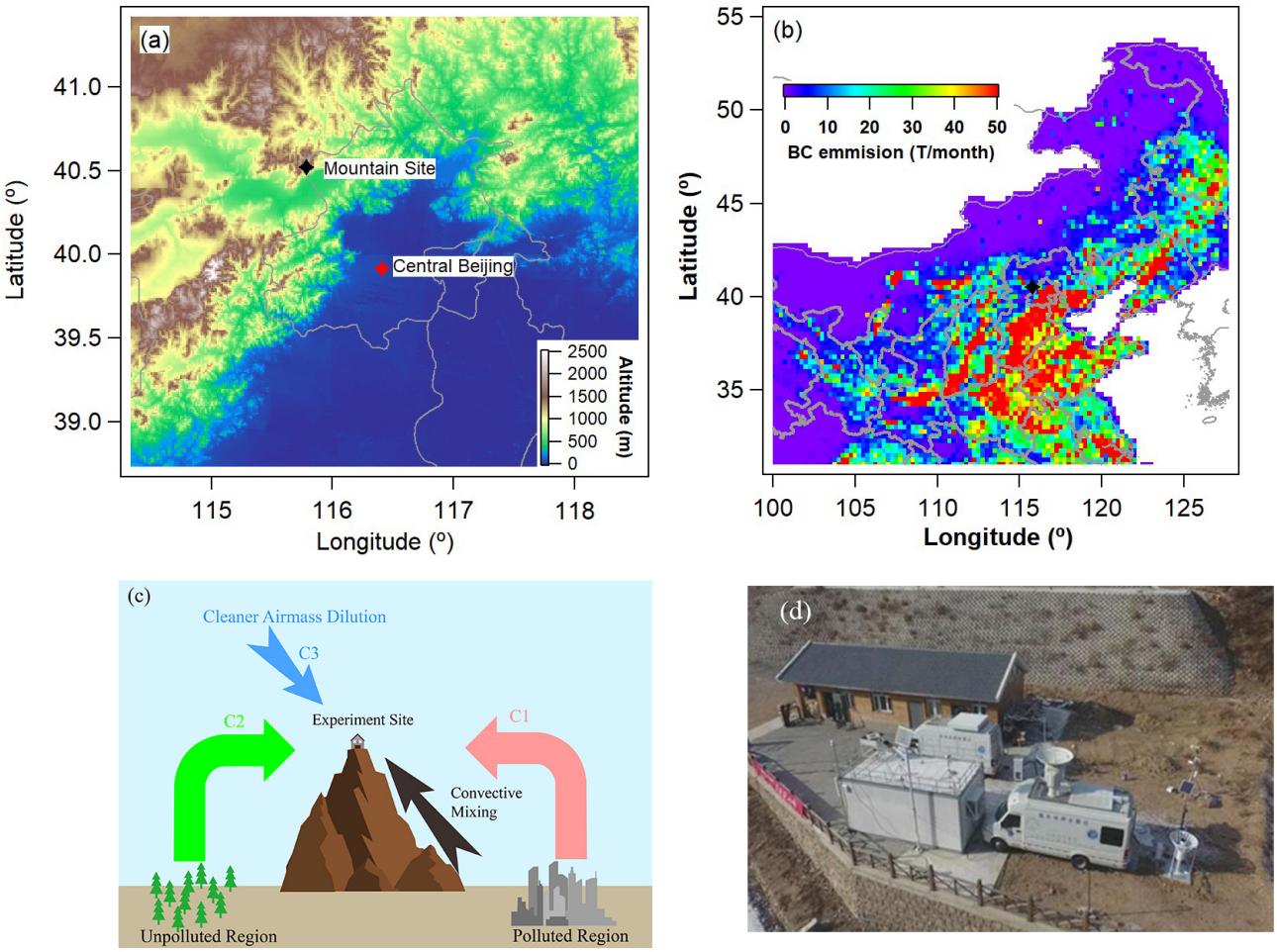

Fig. 1. Experimental site descriptions. (a) The location of the experimental site and central Being, marked with black and red star respectively, where the color bar denotes the terrian height. (b) the monthly BC emission inventory in China (Li et al., 2017). (c) Schematic illustration for different types of PBL defined in this study. (d) Photo of the mountain station.

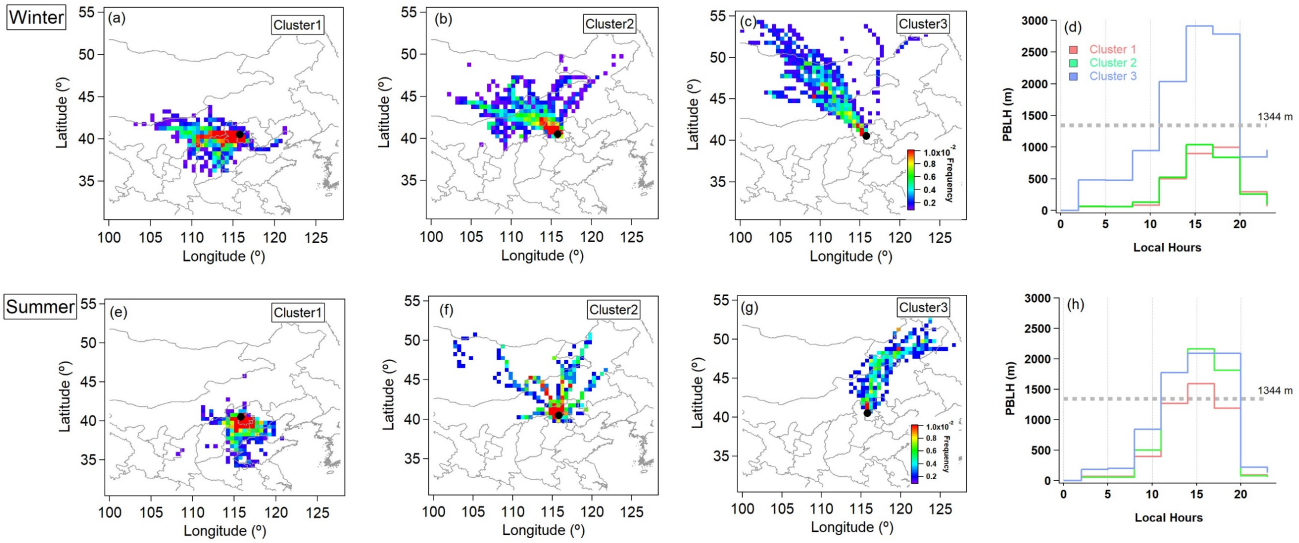

Fig. 2. The clustered backward trajectories from HYSPLIT model in both seasons: (a)-(c) for winter and (e)-(g) for summer, colored by occurrence frequency in each geographic grid. (d) and (h) are the diurnal variation of the height of PBL for the three clusters in both seasons, with the dashed line denoting the mountain site altitude.

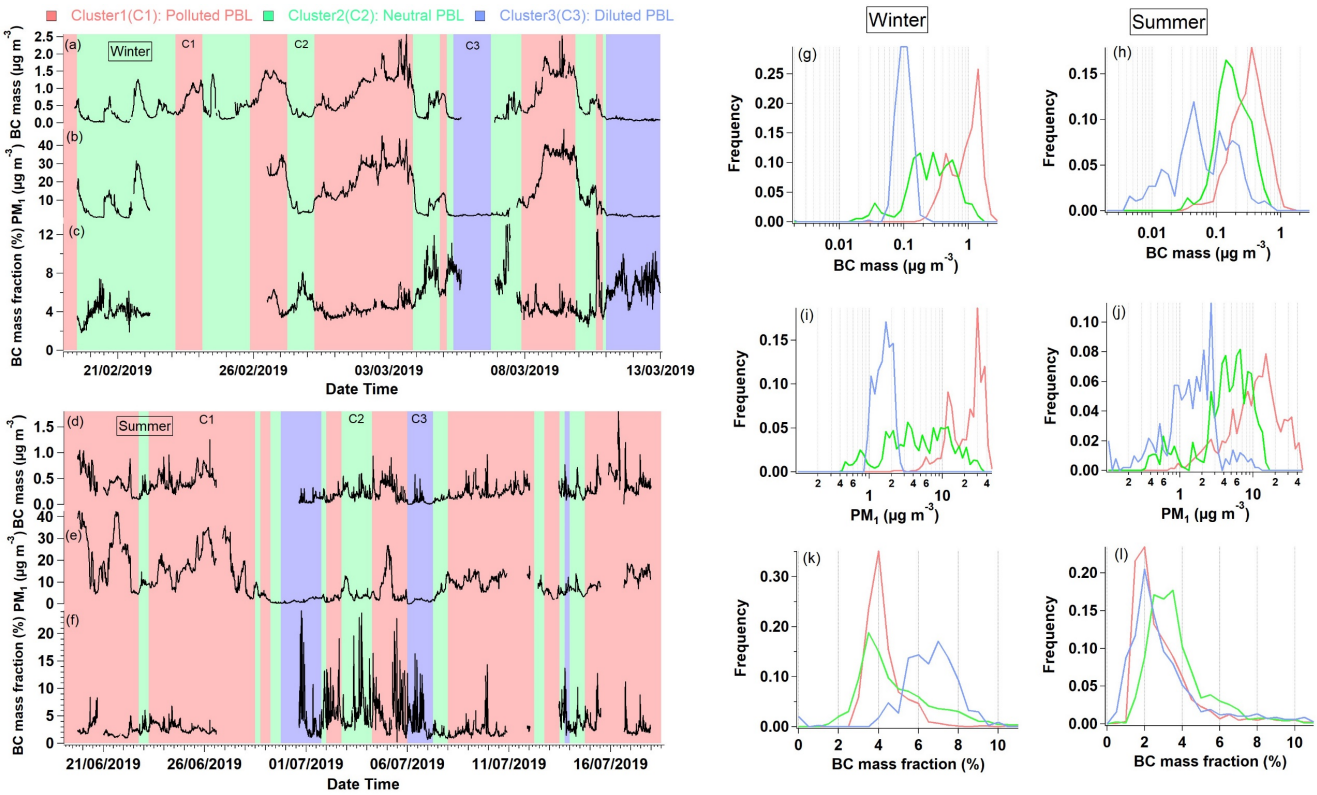

Fig. 3. Time series of BC mass (a)(d), PM_1 derived from the SMPS size distribution (b)(e), BC mass fraction (c)(f) at both seasons, shaded by the periods in identified three clusters, by red, green and blue corresponding to cluster 1 (C1), cluster 2 (C2), cluster 3 (C3) respectively. Frequency histograms of BC mass (g)(h), PM_1 (i)(j), and BC mass fraction (k)(l) for each cluster in both seasons.

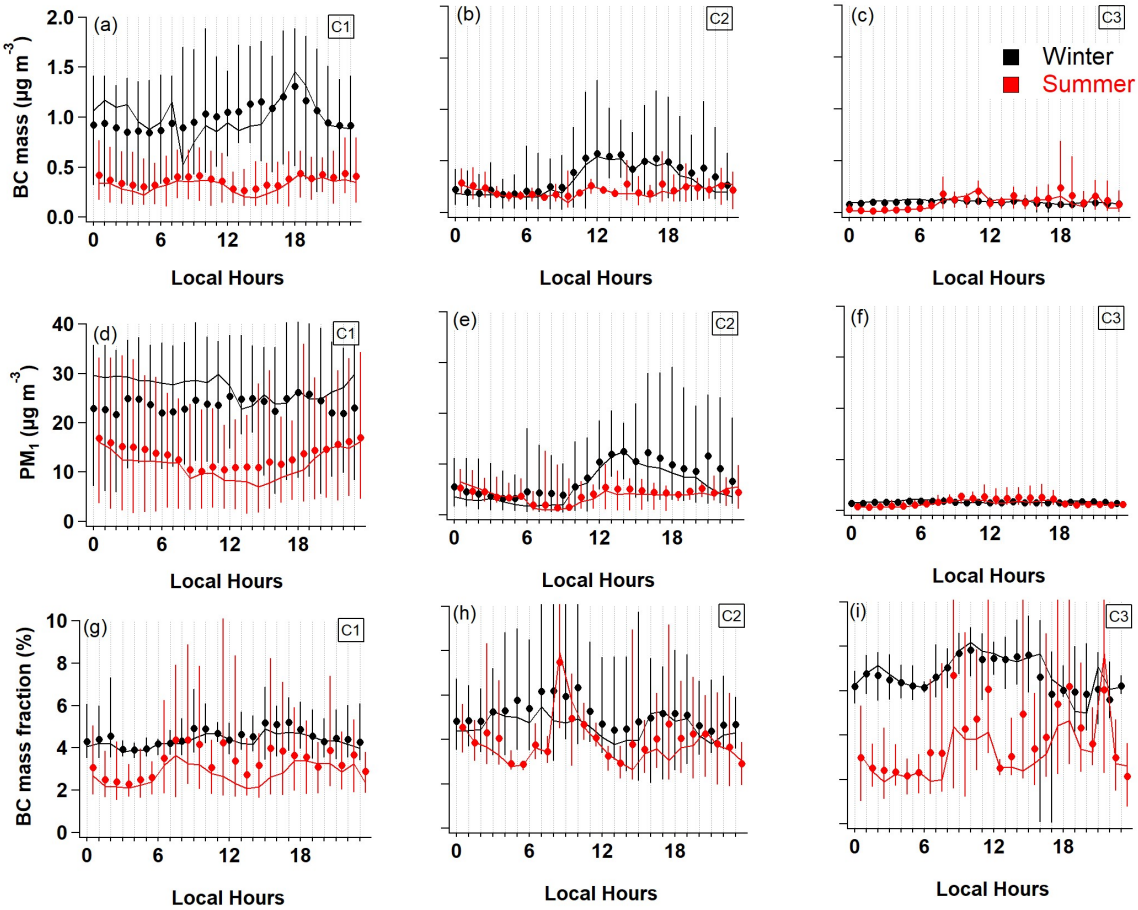

Fig. 4. Diurnal variarion of BC mass (a-c), PM_1 (d-f) and BC mass fraction (g-i) for the three PBL types in both seasons, where black and red denote the winter and summer respectively. The solid circles, lines and whiskers denote the mean, median, 25th, 75th percentile respectively.

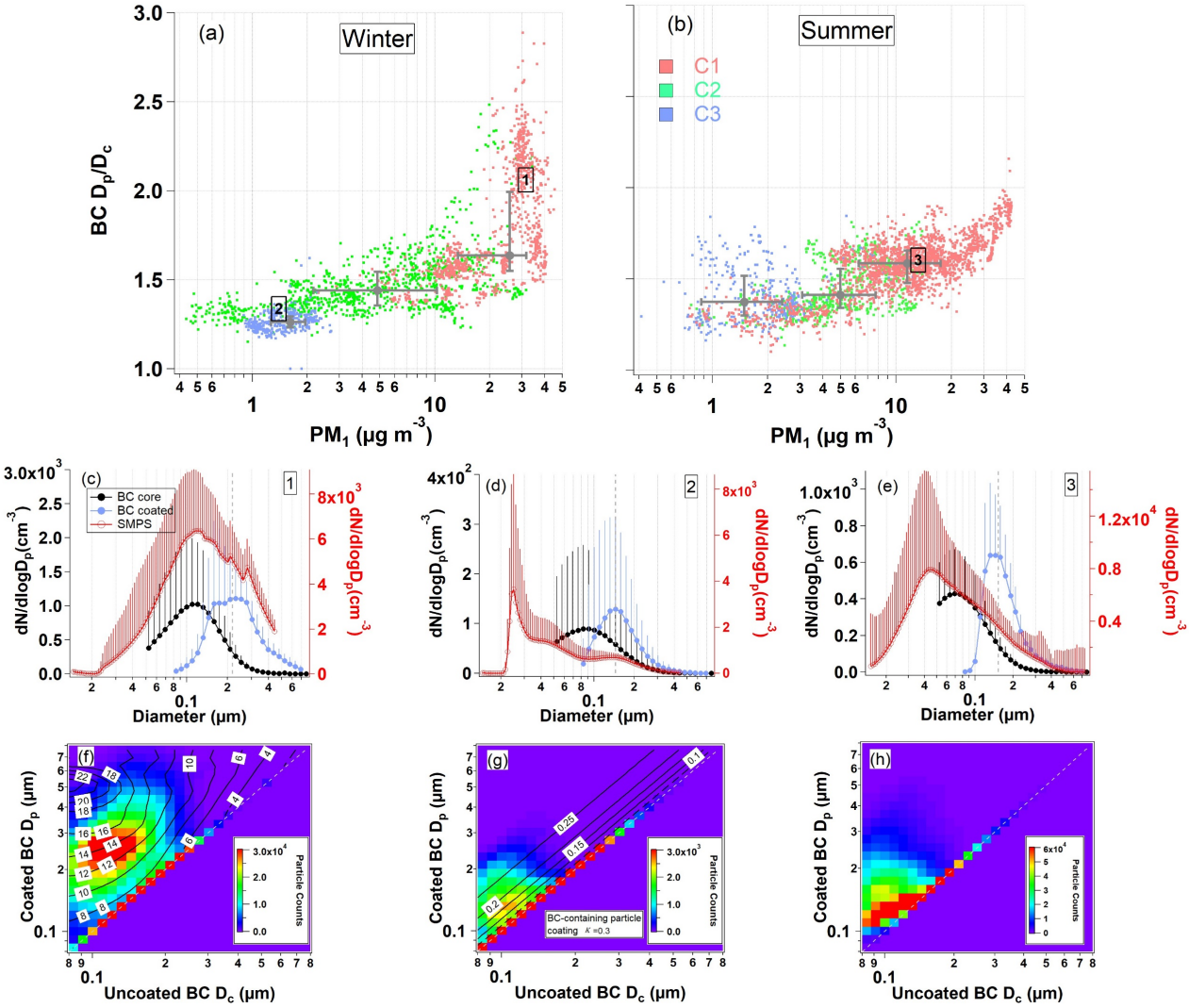

Fig. 5. Size-resolved mixing state of BC. The bulk relative coating thickness (D_p/D_c) as a function of PM_1 in winter (a) and summer (b) for the three PBL types, with solid circles, whiskers denoting the median, 25th, 75th percentiles respectively. Three typical periods, as marked as 1-3 in (a) and (b), are extracted for size distribution analysis. (c),(d) and (e) are the corresponding number size distribution of all particles, uncoated and coated BC for period 1-3 respectively. The bottom panels are coated BC diameter as a function of uncoated BC diameter, colored by number density of single particle, where (f) and (g) are mapped with contour lines numbered by the MAC and κ_{BCc} respectively.

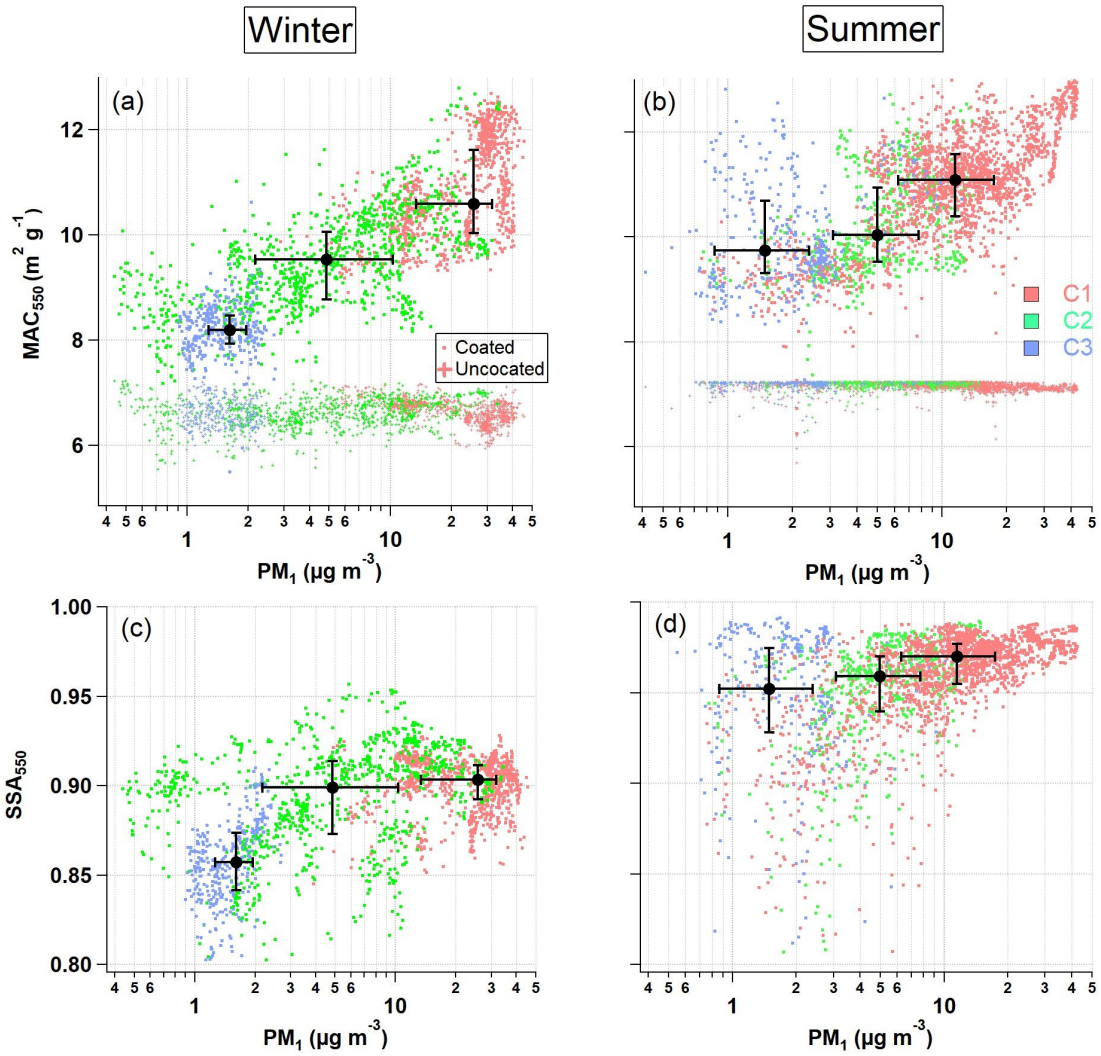

Fig. 6. Optical properties of BC for the three PBL types in both seasons. (a)(b) are mass absorption cross section at λ=550 nm (MAC_{550}), with dot and plus markers denoting coated and uncoated BC respectively. (c)(d) are single-scattering albedo at λ=550 nm (SSA_{550}). In each panel, the solid circles and whiskers denote the median, 25th and 75th percentile respectively.

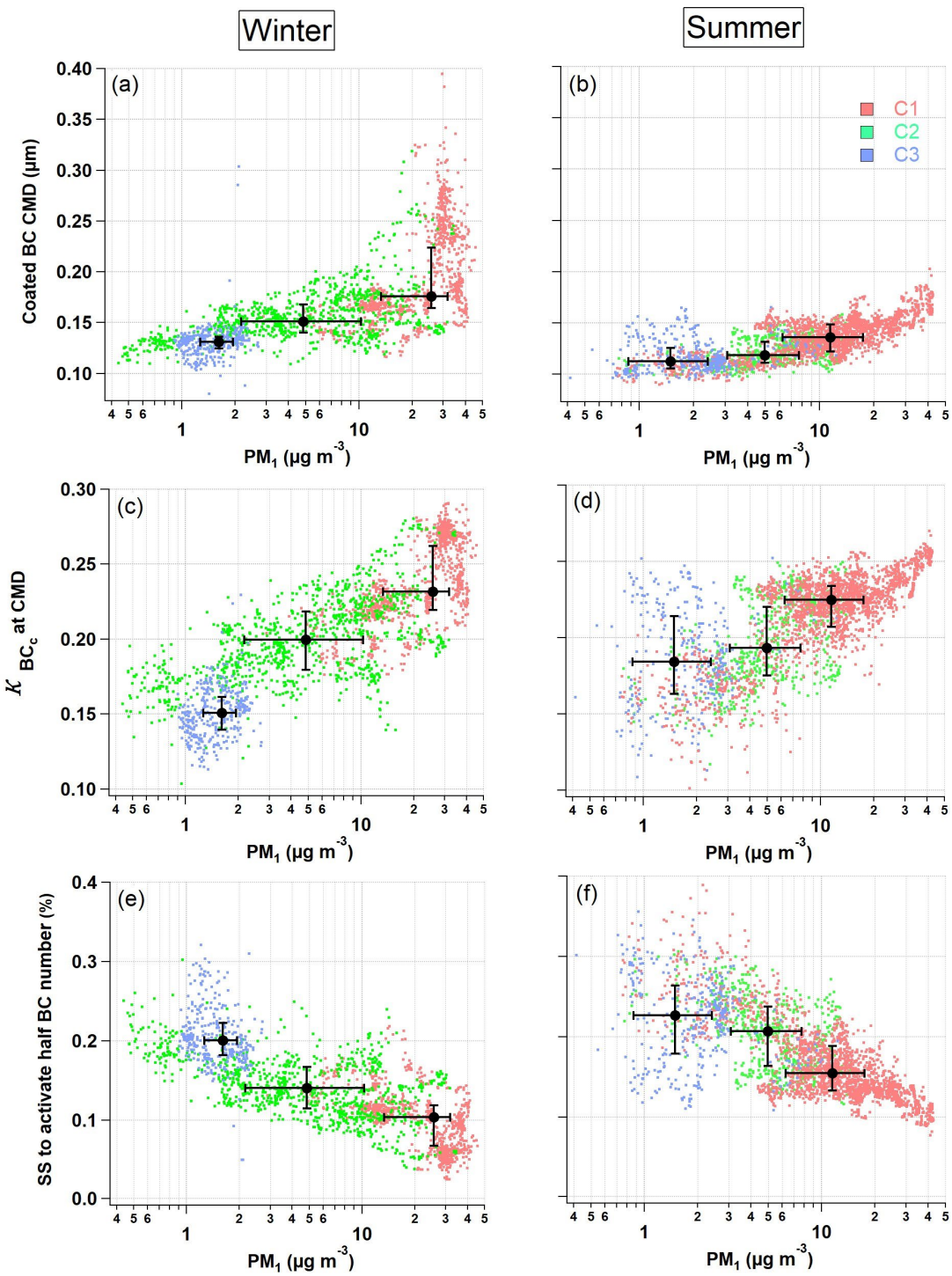

Fig. 7. Hygroscopic properties of BC for the three PBL types in both seasons. (a)(b) are the count median diameter of coated BC; (c)(d) are the κ_{BCc} assuming $\kappa_{coating}$ =0.3; (e)(f) are the supersaturation (SS) to activate half of the BC number population. In each panel, the solid circles and whiskers denote the median, 25th and 75th percentile respectively.

Reference

Adachi, K., and Buseck, P. R.: Changes of ns-soot mixing states and shapes in an urban area during CalNex, Journal of Geophysical Research: Atmospheres, 118, 3723-3730, https://doi.org/10.1002/jgrd.50321, 2013.

Bao, F., Li, M., Zhang, Y., Chen, C., and Zhao, J.: Photochemical Aging of Beijing Urban PM2.5: HONO Production, Environmental

Science & Technology, 52, 6309-6316, 10.1021/acs.est.8b00538, 2018.
Bennett, L. J., Weckwerth, T. M., Blyth, A. M., Geerts, B., Miao, Q., and Richardson, Y.: Observations of the Evolution of the Nocturnal and Convective Boundary Layers and the Structure of Open-Celled Convection on 14 June 2002, Monthly Weather Review, 138, 2589-2607, 2010.
Bohren, C. F., and Huffman, D. R: Absorption and Scattering by a Sphere, in: Absorption and Scattering of Light by Small Particles, 82-129, 1998.
Bond, T. C., and Bergstrom, R.: Light Absorption by Carbonaceous Particles: An Investigative Review, Aerosol Science and Technology, 40, 27-67, 2006.
Bond, T. C., Doherty, S. J., Fahey, D. W., Forster, P. M., Berntsen, T., DeAngelo, B. J., Flanner, M. G., Ghan, S., Kärcher, B., Koch, D., Kinne, S., Kondo, Y., Quinn, P. K., Sarofim, M. C., Schultz, M. G., Schulz, M., Venkataraman, C., Zhang, H., Zhang, S., Bellouin, N., Guttikunda, S. K., Hopke, P. K., Jacobson, M. Z., Kaiser, J. W., Klimont, Z., Lohmann, U., Schwarz, J. P., Shindell, D., Storelvmo, T., Warren, S. G., and Zender, C. S.: Bounding the role of black carbon in the climate system: A scientific assessment, Journal of Geophysical Research: Atmospheres, 118, 5380-5552, 10.1002/jgrd.50171, 2013.
Bretherton, C. S., and Wyant, M. C.: Moisture Transport, Lower-Tropospheric Stability, and Decoupling of Cloud-Topped Boundary Layers, Journal of the Atmospheric Sciences, 54, 148-167, 1997.
Cheng, Y., Su, H., Rose, D., Gunthe, S. S., Berghof, M., Wehner, B., Achtert, P., Nowak, A., Takegawa, N., and Kondo, Y.: Size-resolved measurement of the mixing state of soot in the megacity Beijing, China: diurnal cycle, aging and parameterization, Atmospheric Chemistry and Physics, 12, 4477-4491, 2011.
Chow, J. C., Watson, J. G., Lowenthal, D. H., Antony Chen, L. W., and Motallebi, N.: PM2.5 source profiles for black and organic carbon emission inventories, Atmospheric Environment, 45, 5407-5414, https://doi.org/10.1016/j.atmosenv.2011.07.011, 2011.
Chuang, C. C., Penner, J. E., Prospero, J. M., Grant, K. E., Rau, G. H., and Kawamoto, K.: Cloud susceptibility and the first aerosol indirect forcing: Sensitivity to black carbon and aerosol concentrations, Journal of Geophysical Research, 107, 4564, 2002.
Chung, C. E., Ramanathan, V., and Kiehl, J. T.: Effects of the south Asian absorbing haze on the northeast monsoon and surface-air heat exchange, Journal of Climate, 15, 2462-2476, 2002.
Cross, E. S., and et al.: Laboratory and ambient particle density determinations using light scattering in conjunction with aerosol mass spectrometry, Aerosol Sci. Technol., 41, 343, 2007.
Ding, A., Huang, X., Nie, W., Sun, J., Kerminen, V. M., Petaja, T., Su, H., Cheng, Y., Yang, X., and Wang, M.: Enhanced haze pollution by black carbon in megacities in China, Geophysical Research Letters, 43, 2873-2879, 2016.
Ding, S., Liu, D., Zhao, D., Hu, K., Tian, P., Zhou, W., Huang, M., Yang, Y., Wang, F., and Sheng, J.: Size-Related Physical Properties of Black Carbon in the Lower Atmosphere over Beijing and Europe, Environmental Science & Technology, 53, 11112-11121, 2019a.
Ding, S., Zhao, D., He, C., Huang, M., He, H., Tian, P., Liu, Q., Bi, K., Yu, C., Pitt, J., Chen, Y., Ma, X., Chen, Y., Jia, X., Kong, S., Wu, J., Hu, D., Hu, K., Ding, D., and Liu, D.: Observed Interactions Between Black Carbon and Hydrometeor During Wet Scavenging in Mixed-Phase Clouds, Geophysical Research Letters, 46, 8453-8463, 10.1029/2019gl083171, 2019b.
Draxler, R. R., and Hess, G.: An overview of the HYSPLIT_4 modelling system for trajectories, Aust. Meteorol. Mag., 47, 295, 1998.
Dusek, U., Frank, G., Hildebrandt, L., Curtius, J., Schneider, J., Walter, S., Chand, D., Drewnick, F., Hings, S. S., and Jung, D.: Size matters more than chemistry for cloud-nucleating ability of aerosol particles, Science, 312, 1375-1378, 2006a.
Dusek, U., Reischl, G. P., and Hitzenberger, R.: CCN activation of pure and coated carbon black particles, Environmental Science & Technology, 40, 1223-1230, 2006b.
Gao, R. S., Schwarz, J. P., Kelly, K. K., Fahey, D. W., Watts, L. A., Thompson, T. L., Spackman, J. R., Slowik, J. G., Cross, E. S., and Han, J.: A Novel Method for Estimating Light-Scattering Properties of Soot Aerosols Using a Modified Single-Particle Soot Photometer, Aerosol Science and Technology, 41, 125-135, 2007.
Govardhan, G., Satheesh, S. K., Nanjundiah, R., Moorthy, K. K., and Babu, S. S.: Possible climatic implications of high-altitude black carbon emissions, Atmos. Chem. Phys., 17, 9623-9644, 10.5194/acp-17-9623-2017, 2017.
Grivas, G., Chaloulakou, A., and Kassomenos, P.: An overview of the PM10 pollution problem, in the Metropolitan Area of Athens, Greece. Assessment of controlling factors and potential impact of long range transport, Science of The Total Environment, 389, 165-177, https://doi.org/10.1016/j.scitotenv.2007.08.048, 2008.

Guleria, R. P., Kuniyal, J. C., Dhyani, P. P., Joshi, R. C., and Sharma, N. L.: Impact of aerosol on surface reaching solar irradiance over Mohal in the northwestern Himalaya, India, Journal of Atmospheric and Solar-Terrestrial Physics, 108, 41-49, 2014.

Hallquist, M., Wenger, J. C., Baltensperger, U., Rudich, Y., Simpson, D., Claeys, M., Dommen, J., Donahue, N. M., George, C., and Goldstein, A. H.: The formation, properties and impact of secondary organic aerosol: current and emerging issues, Atmospheric Chemistry and Physics, 9, 5155-5236, 2009.

Han, S., Kondo, Y., Oshima, N., Takegawa, N., Miyazaki, Y., Hu, M., Lin, P., Deng, Z. Z., Zhao, Y., and Sugimoto, N.: Temporal variations of elemental carbon in Beijing, Journal of Geophysical Research, 114, 2009.

Hansen, J., Johnson, D. W., Lacis, A. A., Lebedeff, S., Lee, P., Rind, D., and Russell, G. L.: Climate impact of increasing atmospheric carbon dioxide, Science, 213, 957-966, 1981.

Hansen, J., Sato, M., Ruedy, R., Nazarenko, L., Lacis, A., Schmidt, G. A., Russell, G., Aleinov, I., Bauer, M., Bauer, S., Bell, N., Cairns, B., Canuto, V., Chandler, M., Cheng, Y., Del Genio, A., Faluvegi, G., Fleming, E., Friend, A., Hall, T., Jackman, C., Kelley, M., Kiang, N., Koch, D., Lean, J., Lerner, J., Lo, K., Menon, S., Miller, R., Minnis, P., Novakov, T., Oinas, V., Perlwitz, J., Perlwitz, J., Rind, D., Romanou, A., Shindell, D., Stone, P., Sun, S., Tausnev, N., Thresher, D., Wielicki, B., Wong, T., Yao, M., and Zhang, S.: Efficacy of climate forcings, Journal of Geophysical Research: Atmospheres, 110, 10.1029/2005jd005776, 2005.

Haywood, J. M., and Ramaswamy, V.: Global sensitivity studies of the direct radiative forcing due to anthropogenic sulfate and black carbon aerosols, Journal of Geophysical Research, 103, 6043-6058, 1998.

Holzinger, R., Goldstein, A. H., Hayes, P. L., Jimenez, J. L., and Timkovsky, J.: Chemical evolution of organic aerosol in Los Angeles during the CalNex 2010 study, Atmos. Chem. Phys., 13, 10125-10141, 10.5194/acp-13-10125-2013, 2013.

Hu, K., Zhao, D., Liu, D., Ding, S., Tian, P., Yu, C., Zhou, W., Huang, M., and Ding, D.: Estimating radiative impacts of black carbon associated with mixing state in the lower atmosphere over the northern North China Plain, Chemosphere, 252, 126455, https://doi.org/10.1016/j.chemosphere.2020.126455, 2020.

Jacobson, M. Z.: Investigating cloud absorption effects: global absorption properties of black carbon, tar balls, and soil dust in clouds and aerosols, J. Geophys. Res.: Atmos., 117, 2012.

Ji, D., Yan, Y., Wang, Z., He, J., Liu, B., Sun, Y., Gao, M., Li, Y., Cao, W., Cui, Y., Hu, B., Xin, J., Wang, L., Liu, Z., Tang, G., and Wang, Y.: Two-year continuous measurements of carbonaceous aerosols in urban Beijing, China: Temporal variations, characteristics and source analyses, Chemosphere, 200, 191-200, https://doi.org/10.1016/j.chemosphere.2018.02.067, 2018.

Jorba, O., Perez, C., Rocadenbosch, F., and Baldasano, J. M.: Cluster analysis of 4 day back trajectories arriving in the Barcelona Area (Spain) from 1997 to 2002, Journal of Applied Meteorology, 43, 887-901, 2004.

Koch, D., and Del Genio, A.: Black carbon semi-direct effects on cloud cover: review and synthesis, Atmos. Chem. Phys., 10, 7685, 2010.

Laborde, M., Crippa, M., Tritscher, T., Juranyi, Z., Decarlo, P. F., Temimeroussel, B., Marchand, N., Eckhardt, S., Stohl, A., and Baltensperger, U.: Black carbon physical properties and mixing state in the European megacity Paris, Atmospheric Chemistry and Physics, 13, 5831-5856, 2012.

Li, M., Zhang, Q., Kurokawa, J.-i., Woo, J.-H., He, K., Lu, Z., Ohara, T., Song, Y., Streets, D. G., Carmichael, G. R., Cheng, Y., Hong, C., Huo, H., Jiang, X., Kang, S., Liu, F., Su, H., and Zheng, B.: MIX: a mosaic Asian anthropogenic emission inventory under the international collaboration framework of the MICS-Asia and HTAP, Atmospheric Chemistry and Physics, 17, 935-963, 10.5194/acp-17-935-2017, 2017.

Liu, D., Flynn, M., Gysel, M., Targino, A. C., Crawford, I., Bower, K. N., Choularton, T. W., Juranyi, Z., Steinbacher, M., and Huglin, C.: Single particle characterization of black carbon aerosols at a tropospheric alpine site in Switzerland, Atmospheric Chemistry and Physics, 10, 7389-7407, 2010.

Liu, D., Allan, J., Whitehead, J., Young, D., Flynn, M., Coe, H., McFiggans, G., Fleming, Z. L., and Bandy, B.: Ambient black carbon particle hygroscopic properties controlled by mixing state and composition, Atmospheric Chemistry and Physics, 13, 2015-2029, 10.5194/acp-13-2015-2013, 2013.

Liu, D., Allan, J. D., Young, D. E., Coe, H., Beddows, D., Fleming, Z. L., Flynn, M. J., Gallagher, M. W., Harrison, R. M., Lee, J., Prevot, A. S. H., Taylor, J. W., Yin, J., Williams, P. I., and Zotter, P.: Size distribution, mixing state and source apportionment of black carbon aerosol in London during wintertime, Atmospheric Chemistry and Physics, 14, 10061-10084, 10.5194/acp-14-10061-2014, 2014.

Liu, D., Whitehead, J. D., Alfarra, M. R., Reyesvillegas, E., Spracklen, D. V., Reddington, C. L., Kong, S., Williams, P. I., Ting, Y., and Haslett, S. L.: Black-carbon absorption enhancement in the atmosphere determined by particle mixing state, Nature Geoscience, 10, 184-188, 2017.

Liu, D., Joshi, R., Wang, J., Yu, C., Allan, J. D., Coe, H., Flynn, M., Xie, C., Lee, J. D., and Squires, F.: Contrasting physical properties of black carbon in urban Beijing between winter and summer, Atmospheric Chemistry and Physics, 19, 6749-6769, 2019a.

Liu, D., Zhao, D., Xie, Z., Yu, C., Chen, Y., Tian, P., Ding, S., Hu, K., Lowe, D., and Liu, Q.: Enhanced heating rate of black carbon above the planetary boundary layer over megacities in summertime, Environmental Research Letters, 14, 124003, 2019b.

Liu, P., Zhao, C., Liu, P., Deng, Z., Huang, M., Ma, X., and Tie, X.: Aircraft study of aerosol vertical distributions over Beijing and their optical properties, Tellus Series B-chemical & Physical Meteorology, 61, 756–767, 2009.

Liu, Y., Yan, C., and Zheng, M.: Source apportionment of black carbon during winter in Beijing, Science of The Total Environment, 618, 531-541, https://doi.org/10.1016/j.scitotenv.2017.11.053, 2018.

Liu, Z., Hu, B., Ji, D., Wang, Y., Wang, M., and Wang, Y.: Diurnal and seasonal variation of the PM2.5 apparent particle density in Beijing, China, Atmospheric Environment, 120, 328-338, 2015.

Makra, L., Matyasovszky, I., Guba, Z., Karatzas, K., and Anttila, P.: Monitoring the long-range transport effects on urban PM10 levels using 3D clusters of backward trajectories, Atmospheric Environment, 45, 2630-2641, https://doi.org/10.1016/j.atmosenv.2011.02.068, 2011.

Markou, M. T., and Kassomenos, P.: Cluster analysis of five years of back trajectories arriving in Athens, Greece, Atmospheric Research, 98, 438-457, https://doi.org/10.1016/j.atmosres.2010.08.006, 2010.

Mcfarquhar, G. M., and Wang, H.: Effects of aerosols on trade wind cumuli over the Indian Ocean: Model simulations, Quarterly Journal of the Royal Meteorological Society, 132, 821-843, 2006.

Mcfiggans, G., Artaxo, P., Baltensperger, U., Coe, H., Facchini, M. C., Feingold, G., Fuzzi, S., Gysel, M., Laaksonen, A., and Lohmann, U.: The effect of physical and chemical aerosol properties on warm cloud droplet activation, Atmospheric Chemistry and Physics, 6, 2593-2649, 2005.

Metcalf, A. R., Craven, J. S., Ensberg, J. J., Brioude, J., Angevine, W., Sorooshian, A., Duong, H. T., Jonsson, H. H., Flagan, R. C., and Seinfeld, J. H.: Black carbon aerosol over the Los Angeles Basin during CalNex, Journal of Geophysical Research: Atmospheres, 117, https://doi.org/10.1029/2011JD017255, 2012.

Nair, V. S., Babu, S. S., Moorthy, K. K., Sharma, A. K., Marinoni, A., and Ajai: Black carbon aerosols over the Himalayas: direct and surface albedo forcing, Tellus B: Chemical and Physical Meteorology, 65, 19738, 10.3402/tellusb.v65i0.19738, 2013.

Nenes, A., and et al.: Black carbon radiative heating effects on cloud microphysics and implications for the aerosol indirect effect 2. Cloud microphysics, J. Geophys. Res.: Atmos., 107, 4605, 2002.

Panicker, A. S., Pandithurai, G., Safai, P. D., and Prabha, T. V.: Indirect forcing of black carbon on clouds over northeast India, Quarterly Journal of the Royal Meteorological Society, 142, 2968-2973, 10.1002/qj.2878, 2016.

Philipp, A.: Comparison of principal component and cluster analysis for classifying circulation pattern sequences for the European domain, Theoretical and Applied Climatology, 96, 31-41, 2009.

Pringle, K. J., Tost, H., Pozzer, A., Pöschl, U., and Lelieveld, J.: Global distribution of the effective aerosol hygroscopicity parameter for CCN activation, Atmospheric Chemistry and Physics, 10, 5241-5255, 10.5194/acp-10-5241-2010, 2010.

Pruppacher, H. R., Klett, J. D., and Wang, P. K.: Microphysics of Clouds and Precipitation, Aerosol Science and Technology, 28, 381-382, 10.1080/02786829808965531, 1998.

Raju, M. P., Safai, P. D., Sonbawne, S. M., Buchunde, P. S., Pandithurai, G., and Dani, K. K.: Black carbon aerosols over a high altitude station, Mahabaleshwar: Radiative forcing and source apportionment, Atmospheric Pollution Research, 11, 1408-1417, https://doi.org/10.1016/j.apr.2020.05.024, 2020.

Ramanathan, V., Chung, C. E., Kim, D., Bettge, T. W., Buja, L., Kiehl, J. T., Washington, W. M., Fu, Q., Sikka, D., and Wild, M.: Atmospheric brown clouds: Impacts on South Asian climate and hydrological cycle, Proceedings of the National Academy of Sciences of the United States of America, 102, 5326-5333, 2005.

Ramanathan, V., and Carmichael, G.: Global and regional climate changes due to black carbon, Nat. Geosci., 1, 221, 2008.

Rudich, Y., Sagi, A., and Rosenfeld, D.: Influence of the Kuwait oil fires plume (1991) on the microphysical development of clouds, Journal of Geophysical Research, 108, 10.1029/2003JD003472, 2003.

Schwarz, J. P., Gao, R. S., Fahey, D. W., Thomson, D. S., Watts, L. A., Wilson, J. C., Reeves, J. M., Darbeheshti, M., Baumgardner, D., and Kok, G. L.: Single-particle measurements of midlatitude black carbon and light-scattering aerosols from the boundary layer to the lower stratosphere, Journal of Geophysical Research, 111, 2006.

Srivastava, A., Ram, K., Pant, P., Hegde, P., and Joshi, H.: Black carbon aerosols over Manora Peak in the Indian Himalayan foothills: implications for climate forcing, Environmental Research Letters, 7, 014002, 2012a.

Srivastava, A. K., Singh, S., Pant, P., and Dumka, U. C.: Characteristics of black carbon over Delhi and Manora Peak—a comparative study, Atmospheric Science Letters, 13, 223-230, 10.1002/asl.386, 2012b.

Srivastava, P., Dey, S., Srivastava, A. K., Singh, S., and Tiwari, S.: Most probable mixing state of aerosols in Delhi NCR, northern India, Atmospheric Research, 200, 88-96, https://doi.org/10.1016/j.atmosres.2017.09.018, 2018.

Stokes, R. H., and Robinson, R. A.: Interactions in Aqueous Nonelectrolyte Solutions. I. Solute-Solvent Equilibria, The Journal of Physical Chemistry, 70, 2126-2131, 1966.

Sullivan, P. P., Moeng, C., Stevens, B., Lenschow, D. H., and Mayor, S. D.: Structure of the Entrainment Zone Capping the Convective Atmospheric Boundary Layer, Journal of the Atmospheric Sciences, 55, 3042-3064, 1998.

Tian, P., Liu, D., Zhao, D., Yu, C., Liu, Q., Huang, M., Deng, Z., Ran, L., Wu, Y., Ding, S., Hu, K., Zhao, G., Zhao, C., and Ding, D.: In situ vertical characteristics of optical properties and heating rates of aerosol over Beijing, Atmospheric Chemistry and Physics, 20, 2603-2622, 10.5194/acp-20-2603-2020, 2020.

Volkamer, R., Jimenez, J. L., Martini, F. S., Dzepina, K., Zhang, Q., Salcedo, D., Molina, L. T., Worsnop, D. R., and Molina, M. J.: Secondary organic aerosol formation from anthropogenic air pollution: Rapid and higher than expected, Geophysical Research Letters, 33, 2006.

Weinzierl, B.: Radiatively-driven processes in forest fire and desert dust plumes, DLR Deutsches Zentrum fur Luft- und Raumfahrt e.V. - Forschungsberichte, 2008.

Wood, R., and Bretherton, C. S.: Boundary Layer Depth, Entrainment, and Decoupling in the Cloud-Capped Subtropical and Tropical Marine Boundary Layer, Journal of Climate, 17, 3576-3588, 2004.

Wu, Y., Liu, D., Wang, J., Shen, F., Chen, Y., Cui, S., Ge, S., Wu, Y., Chen, M., and Ge, X.: Characterization of Size-Resolved Hygroscopicity of Black Carbon-Containing Particle in Urban Environment, Environmental Science & Technology, 53, 14212-14221, 10.1021/acs.est.9b05546, 2019.

Xu, W., Han, T., Du, W., Wang, Q., Chen, C., Zhao, J., Zhang, Y., Li, J., Fu, P., Wang, Z., Worsnop, D. R., and Sun, Y.: Effects of Aqueous-Phase and Photochemical Processing on Secondary Organic Aerosol Formation and Evolution in Beijing, China, Environmental Science & Technology, 51, 762-770, 10.1021/acs.est.6b04498, 2017.

Yang, W., Zhang, Y., Wang, X., Li, S., Zhu, M., Yu, Q., Li, G., Huang, Z., Zhang, H., Wu, Z., Song, W., Tan, J., and Shao, M.: Volatile organic compounds at a rural site in Beijing: Influence of temporary emission control and wintertime heating, Atmospheric Chemistry and Physics Discussions, 1-55, 10.5194/acp-2018-29, 2018a.

Yang, X., Xu, J., Bi, F., Zhang, Z., Chen, Y., He, Y., Han, F., Zhi, G., Liu, S., and Meng, F.: Aircraft measurement over the Gulf of Tonkin capturing aloft transport of biomass burning, Atmospheric Environment, 182, 41-50, https://doi.org/10.1016/j.atmosenv.2018.03.020, 2018b.

Zhang, Y., Zhang, Q., Cheng, Y., Su, H., Li, H., Li, M., Zhang, X., Ding, A., and He, K.: Amplification of light absorption of black carbon associated with air pollution, Atmospheric Chemistry and Physics, 18, 9879-9896, 2018.

Zhao, D., Huang, M., Tian, P., He, H., Lowe, D., Zhou, W., Sheng, J., Wang, F., Bi, K., Kong, S., Yang, Y., Liu, Q., Liu, D., and Ding, D.: Vertical characteristics of black carbon physical properties over Beijing region in warm and cold seasons, Atmospheric Environment, 213, 296-310, https://doi.org/10.1016/j.atmosenv.2019.06.007, 2019.